

IDETC2019-97427

ON THE DEPLOYMENT OF MULTISTABLE KRESLING ORIGAMI-INSPIRED STRUCTURES

Narayanan Kidambi, K.W. Wang

Department of Mechanical Engineering, University of Michigan
Ann Arbor, MI, USA 48109

ABSTRACT

Origami designs have attracted significant attention from researchers seeking to develop new types of deployable structures due to their ability to undergo large and complex yet predictable shape changes. The Kresling pattern, which is based on a natural accumulation of folds and creases during the twist-buckling of a thin-walled cylinder, offers a great example for the design of deployable systems that expand uniaxially into tubes or booms. However, much remains to be understood regarding the characteristics of Kresling-based deployable systems, and their dynamics during the deployment process remain largely unexplored. Hence this research investigates the deployment of Kresling origami-inspired structures, employing a full six-degree-of-freedom truss-based model to study their dynamics under different conditions. Results show that tuning the initial rotation angle of a structure gives rise to several qualitatively distinct mechanical properties and stability characteristics, each of which has different implications for the design of the deployable systems. Dynamic analyses reveal the robustness of Kresling structures to out-of-axis perturbations while remaining compliant in the axial direction. These findings suggest that Kresling-based designs can form the basis for the development of new types of deployable structures and systems with tunable performance.

INTRODUCTION

Origami, a traditional paper-folding art form, transforms a flat sheet of material into complex 3D objects through careful design of crease folding patterns, opening up a vast design space for range of engineering applications. Origami designs have the potential to achieve large-scale shape-change as the crease fold angles are varied, offering great inspiration for the design of deployable or shape-morphing structures. Such structures can be assembled, stowed, and/or transported in a space-saving flat configuration before being deployed into their larger operational configuration when needed [1,2]. This approach has led to novel

concepts for origami-inspired self-assembling robots [3], deployable space booms [4], solar arrays [5], and shelters [6].

Significant progress has been made on the design and analysis of deployable structures based on tube-like compositions of origami due to their ability to bear loads [7], change stiffness [8,9], and the natural application of such designs for shelters and enclosures [4,6]. Among the most widely-studied origami designs that give rise to such features is the well-known Miura pattern [5]. Interleaving or connecting multiple Miura tubes enables significant volume change and anisotropic stiffness adaptivity [10,11]. The Miura pattern is rigidly foldable, which means that the flat facets remain undeformed during the folding or morphing process, and can hence be modeled as rigid panels [12]. Non-rigid foldable designs, on the other hand, result in bending and/or stretching deformations of the facets during shape change [13]. Several non-rigid folding patterns draw inspiration from physical or biological phenomena [14]. A thin walled cylinder subject to axial loads will buckle to a topology that resembles an arrangement of triangular faces [15]. This observation has led to the study of cylindrical origami structures with crease patterns that reflect this topology, giving rise to non-monotonic stiffness responses as portions of the structure collapse [16]. When thin-walled cylinders are subject to twist-buckling, they exhibit a similar behavior, though with discrete layers of triangular facets oriented in the same direction. Origami crease patterns based on this phenomenon are known as Kresling patterns [17,18].

Multiple Kresling modules can be serially assembled, forming larger, more complex, multistable structures that may be deployed to one of its many stable lengths. This is illustrated by the commercially available wine bag (Origami Wine Tote, BUILT NY, USA) depicted in Figure 1. Due to the non-rigid foldability of this pattern, a transition from the collapsed to the deployed state of each module requires the triangular facets to bend and stretch. This means that traditional kinematic models of rigid origami folding cannot be directly employed. Researchers have thus adopted various approaches such as



FIGURE 1. ORIGAMI WINE TOTE (BUILT NY, USA) CONSTRUCTED FROM MULTIPLE KRESLING LAYERS, SHOWING STABLE INTERMEDIATE CONFIGURATIONS FROM LEFT TO RIGHT AS EACH SUCCESSIVE LAYER IS COLLAPSED FROM ITS EXPANDED STATE.

adding virtual folds that change position and orientation during the deployment process [19], or treating the creases as bars or trusses that may change length and store energy [13]. Kresling-based truss structures have been shown to demonstrate tunable stiffness behaviors depending on geometric parameters, and possess the ability to bear loads by naturally locking into a deployed state [7,20]. Such features, combined with the ability to fold into a compact, flat configuration, make the Kresling pattern an appealing platform for the development of deployable structures [21].

While past research suggests strong potential for Kresling-inspired deployable structures, the behavior of such structures during the deployment process remains to be fully understood. These behaviors may be rather complex, as the snap-through motions of bistable layers between the collapsed and deployed states is expected to generate fast dynamic behaviors that depend strongly on the structure's geometry. Furthermore, prior investigations of Kresling structures have treated each module as a two degree-of-freedom (2 DOF) system. Only axial displacements and rotations considered while other degrees of freedom are physically constrained [22]. On the other hand, examinations of physical realizations of the Kresling architecture that do not possess such additional constraints, such as the specimen pictured in Figure 1, suggest that out-of-axis deformations can occur and need to be considered. Such motions may arise if the structure is subject to perturbations and disturbances that are not perfectly aligned with the deployment axis, or if there are manufacturing imperfections that compromise the symmetry of the structure. This is especially important if the deployable Kresling structure is intended to protect sensitive equipment, as has been proposed for certain applications [21].

The goals of this research are to advance the state of the art through, for the first time, investigations of the dynamic responses of Kresling-based truss structures during their deployment process, and to provide good insight to design them as effective and robust deployable structures by explicitly considering out-of-axis motions. First, a full, 6 DOF truss model of a Kresling module is developed using a Newton-Euler approach. The influence of geometric parameters on multistability and energy barriers between stable states is then

discussed, followed by an investigation of different dynamic deployment scenarios. Lastly, the performance of Kresling structures under off-axis perturbations is examined, aided by an analysis of their normal modes in the deployed configuration.

MODEL FORMULATION

This research adopts a truss-based representation of a Kresling module [7,8], as depicted in Figure 2. The top and bottom faces are represented as two rigid regular n -sided polygons with mass m , circumscribed by a circle with radius R_0 . The module has a natural height h_0 and rotation γ_0 for which all the truss elements, shown by dashed or dotted lines, have zero strain. There are two sets of truss elements. *Vertical* trusses, denoted by dashed lines, connect node A_i on the lower surface with node B_i on the upper surface, while *diagonal* trusses,

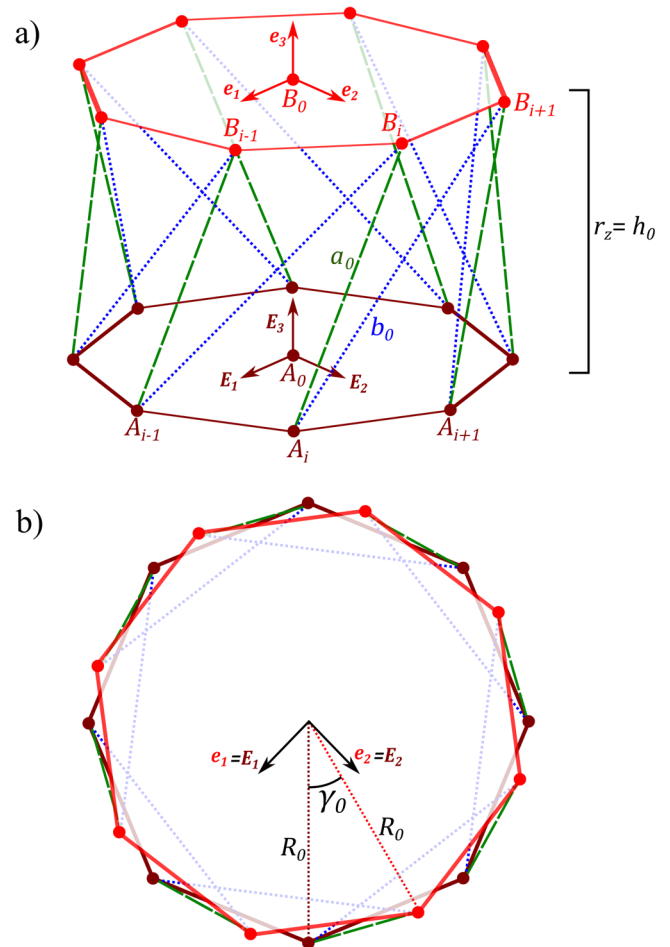


FIGURE 2. (a) PERSPECTIVE VIEW OF A KRESLING MODULE. TWO n -SIDED POLYGONS ARE CIRCUMSCRIBED BY CIRCLES WITH RADIUS R_0 . THE VERTICES ARE CONNECTED BY VERTICAL AND DIAGONAL TRUSSES WITH NATURAL LENGTHS a_0 AND b_0 , RESPECTIVELY. (b) TOP VIEW, SHOWING THAT IN THE UNDEFORMED STATE, THE UPPER LAYER IS ROTATED BY AN ANGLE γ_0 WITH RESPECT TO THE LOWER LAYER. COORDINATE SYSTEMS $[E_1, E_2, E_3]$ AND $[e_1, e_2, e_3]$ ARE ATTACHED TO THE TWO PLATES.

denoted by dotted lines connect node A_i with node B_{i+1} , for $i \in \{1 \dots n\}$. At the module's initial height h_0 , the vertical trusses have an unstretched length of a_0 while the diagonal trusses have an unstretched length b_0 . A set of space-fixed orthonormal coordinate vectors, $[\mathbf{E}_1, \mathbf{E}_2, \mathbf{E}_3]$ is fixed to the A_0 , the center of the lower plate. A set of body-fixed coordinate vectors $[\mathbf{e}_1, \mathbf{e}_2, \mathbf{e}_3]$ is attached to B_0 , the center of the upper plate.

Figure 3 shows the Kresling module with some prescribed height r_z and rotation γ about \mathbf{E}_3 . Under these prescribed conditions, the vertical and diagonal trusses deform to a length a and b , respectively. For a given r_z , the corresponding total rotation $\gamma + \gamma_0$ may minimize the energy stored in the trusses, though this does not imply that the trusses are undeformed [18]. In other words, the trusses generally exhibit some strain in order to accommodate the prescribed height and rotation, such that $a \neq a_0$ and $b \neq b_0$.

Under pure uniaxial compression with rotation about the same axis, all vertical and diagonal trusses deform identically. However, one of the present research goals is to investigate the off-axis dynamics of Kresling structures. Thus, a suitable model needs to preserve all degrees of freedom. Figure 4 presents a schematic of a Kresling module with an arbitrary orientation, and

where the vertical and diagonal trusses are not identically deformed.

The center of mass B_0 of the upper layer has a position vector \mathbf{r}_{B_0/A_0} with respect to the origin A_0 . This vector is expressed in space-fixed coordinates as:

$$\mathbf{r}_{B_0/A_0} = r_x \mathbf{E}_1 + r_y \mathbf{E}_2 + r_z \mathbf{E}_3 \quad (1)$$

The body fixed coordinate system $[\mathbf{e}_1, \mathbf{e}_2, \mathbf{e}_3]$ is related to $[\mathbf{E}_1, \mathbf{E}_2, \mathbf{E}_3]$ through a rotation tensor \mathbf{R} .

$$\mathbf{e}_i = \mathbf{R} \mathbf{E}_i \quad (2)$$

$\forall i \in \{1,2,3\}$. The rotation tensor is constructed using a set of Euler angles, which describes an arbitrary orientation of a rigid body through a sequence of three chained rotations. Here, a set of 3-2-1 Euler angles $\Theta = [\gamma, \beta, \alpha]^T$ is employed [23]. The first of the chained rotations rotates the coordinate system around \mathbf{E}_3 by an angle γ , and has the following matrix representation in the space-fixed frame.

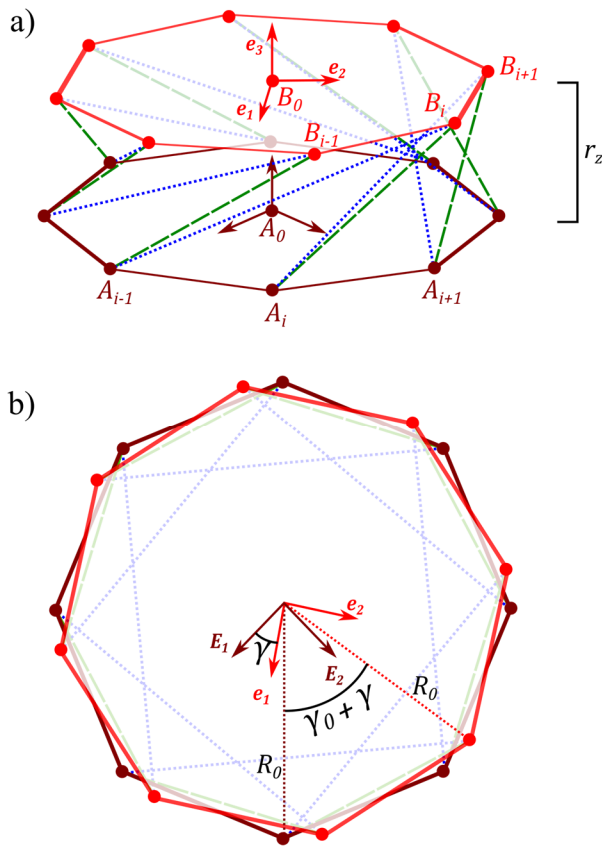


FIGURE 3. (a) PERSPECTIVE VIEW AND (b) TOP VIEW OF A KRESLING MODULE UNDER COMPRESSION WITH HEIGHT r_z . IN THIS COMPRESSED STATE, THE UPPER PLATE IS ROTATED BY AN ANGLE γ WITH RESPECT TO THE UNDEFORMED STATE SHOWN IN FIGURE 2.

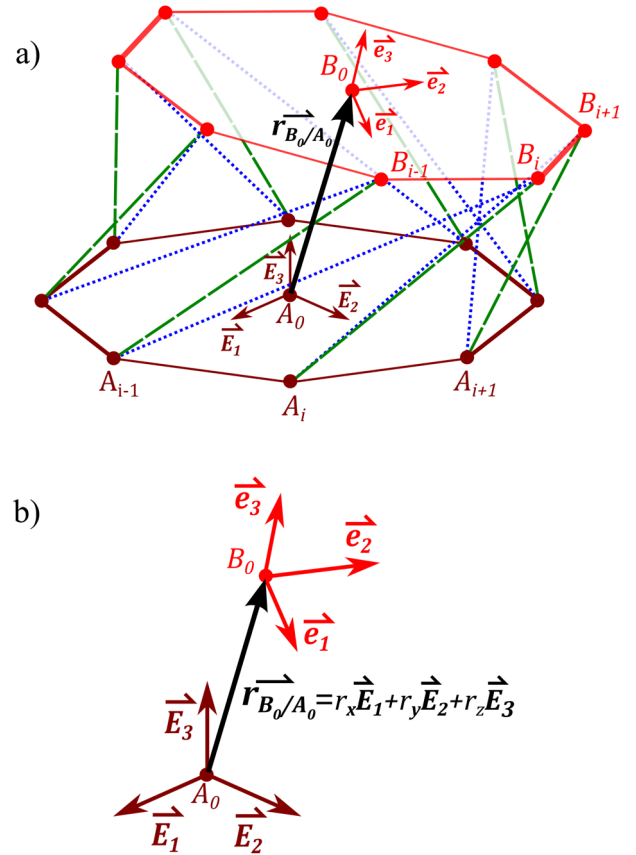


FIGURE 4. (a) PERSPECTIVE VIEW OF A KRESLING MODULE WITH AN ARBITRARY DISPLACEMENT AND ORIENTATION. THE MASS CENTER OF THE UPPER PLATE HAS A POSITION \mathbf{r}_{B_0/A_0} . (b) THE CENTER OF MASS B_0 OF THE UPPER BODY HAS POSITION $r_x \mathbf{E}_1 + r_y \mathbf{E}_2 + r_z \mathbf{E}_3$ IN THE SPACE-FIXED FRAME.

$$\mathbf{R}_1 = \begin{bmatrix} \cos \gamma & -\sin \gamma & 0 \\ \sin \gamma & \cos \gamma & 0 \\ 0 & 0 & 1 \end{bmatrix} \quad (3a)$$

Then, a rotation of angle β is performed around the \mathbf{E}_2' axis, where $\mathbf{E}_2' = \mathbf{R}_1^T \mathbf{E}_2$, and is described by the rotation tensor \mathbf{R}_2 . This is followed by a rotation of α around \mathbf{E}_1'' , where $\mathbf{E}_1'' = (\mathbf{R}_1 \mathbf{R}_2)^T \mathbf{E}_1$. These two rotations may be written in the space-fixed frame as:

$$\mathbf{R}_2 = \begin{bmatrix} \cos \beta & 0 & \sin \beta \\ 0 & 1 & 0 \\ -\sin \beta & 0 & \cos \beta \end{bmatrix} \quad (3b)$$

$$\mathbf{R}_3 = \begin{bmatrix} 1 & 0 & 0 \\ 0 & \cos \alpha & -\sin \alpha \\ 0 & \sin \alpha & \cos \alpha \end{bmatrix} \quad (3c)$$

and yields the following expression for the overall rotation \mathbf{R} :

$$\mathbf{R} = \mathbf{R}_1 \mathbf{R}_2 \mathbf{R}_3 \quad (4)$$

Each of the vertical and diagonal trusses is modeled as a linear elastic spring in parallel with a viscous damper. The total force exerted at point B_i by the two connecting trusses is hence:

$$\begin{aligned} \mathbf{F}_{B_i} = & -k_a (|\mathbf{r}_{B_i/A_i}| - a_0) \hat{\mathbf{r}}_{B_i/A_i} - k_b (|\mathbf{r}_{B_i/A_{i-1}}| - \\ & b_0) \hat{\mathbf{r}}_{B_i/A_{i-1}} - c_a (\dot{\mathbf{r}}_{B_i/A_i} \cdot \hat{\mathbf{r}}_{B_i/A_i}) \hat{\mathbf{r}}_{B_i/A_i} - c_b (\dot{\mathbf{r}}_{B_i/A_{i-1}} \cdot \\ & \hat{\mathbf{r}}_{B_i/A_{i-1}}) \hat{\mathbf{r}}_{B_i/A_{i-1}} \end{aligned} \quad (5)$$

where \mathbf{r}_{B_i/A_i} and $\dot{\mathbf{r}}_{B_i/A_i}$ are the relative position and velocity of node B_i with respect to node A_i , the circumflex symbol ($\hat{\cdot}$) denotes a unit vector, k_a and k_b are the spring constants, and c_a and c_b are the damping coefficients of the vertical and diagonal trusses, respectively. The relative position vector is expressed as the sum:

$$\mathbf{r}_{B_i/A_i} = \mathbf{r}_{B_0/A_0} + \mathbf{r}_{B_i/B_0} - \mathbf{r}_{A_i/A_0} \quad (6)$$

where \mathbf{r}_{A_i/A_0} is the position of each node A_i on the lower n -sided polygonal plate and:

$$\mathbf{r}_{A_i/A_0} = R_0 \cos\left(\frac{2\pi}{n}i\right) \mathbf{E}_1 + R_0 \sin\left(\frac{2\pi}{n}i\right) \mathbf{E}_2 \quad (7)$$

$\forall i \in \{1 \dots n\}$. Similarly, \mathbf{r}_{B_i/B_0} is the position of each node on plate B with respect to its center of mass, and the rotation tensor is employed to yield its position in the space-fixed frame.

$$\mathbf{r}_{B_i/B_0} = R_0 \cos\left(\frac{2\pi}{n}i + \gamma_0\right) \mathbf{e}_1 + R_0 \sin\left(\frac{2\pi}{n}i + \gamma_0\right) \mathbf{e}_2 \quad (8a)$$

$$= \left(\mathbf{R} \begin{bmatrix} R_0 \cos\left(\frac{2\pi}{n}i + \gamma_0\right) \\ R_0 \sin\left(\frac{2\pi}{n}i + \gamma_0\right) \\ 0 \end{bmatrix} \right)^T \begin{bmatrix} \mathbf{E}_1 \\ \mathbf{E}_2 \\ \mathbf{E}_3 \end{bmatrix} \quad (8b)$$

Since the lower plate A is stationary, the relative velocity vector $\dot{\mathbf{r}}_{B_i/A_i}$ is

$$\dot{\mathbf{r}}_{B_i/A_i} = \dot{\mathbf{r}}_{B_0/A_0} + \dot{\mathbf{r}}_{B_i/B_0} \quad (9a)$$

$$= \dot{r}_x \mathbf{E}_1 + \dot{r}_y \mathbf{E}_2 + \dot{r}_z \mathbf{E}_3 + \boldsymbol{\omega}_B \times \mathbf{r}_{B_i/B_0} \quad (9b)$$

where $\boldsymbol{\omega}_B$ is the angular velocity of plate B. Since the Euler basis vectors are generally not orthogonal, the angular velocity is related to Euler angle rates $\dot{\boldsymbol{\Theta}} = [\dot{\gamma}, \dot{\beta}, \dot{\alpha}]^T$ through an appropriate combination of the individual transformations in Equation 3(a-c). In space-fixed coordinates, this may be written as:

$$\boldsymbol{\omega}_B = \mathbf{R}_{\omega_B} \dot{\boldsymbol{\Theta}} = \begin{bmatrix} 0 & -\sin \gamma & \cos \beta \cos \gamma \\ 0 & \cos \gamma & \cos \beta \sin \gamma \\ 1 & 0 & \sin \beta \end{bmatrix} \dot{\boldsymbol{\Theta}} \quad (10)$$

The torque exerted by the force \mathbf{F}_{B_i} about B_0 is

$$\mathbf{T}_{B_i} = \mathbf{r}_{B_i/B_0} \times \mathbf{F}_{B_i} \quad (11)$$

Hence, the translational and rotational accelerations, $\ddot{\mathbf{r}}_{B_0/A_0}$ and $\dot{\boldsymbol{\omega}}_B$ are:

$$\ddot{\mathbf{r}}_{B_0/A_0} = \frac{1}{m_B} \sum_{i=1}^n \mathbf{F}_{B_i} \quad (12a)$$

$$\dot{\boldsymbol{\omega}}_B = (\mathbf{R}^T \mathbf{I}_{B_0} \mathbf{R})^{-1} (\sum_{i=1}^n \mathbf{T}_{B_i} - \boldsymbol{\omega}_B \times (\mathbf{R}^T \mathbf{I}_{B_0} \mathbf{R}) \boldsymbol{\omega}_B) \quad (12b)$$

where m_B is the mass of plate B, and \mathbf{I}_{B_0} is its inertia tensor about B_0 . A thin, circular plate is considered here, with radius R_0 that circumscribes the n -sided polygon. Thus, \mathbf{I}_{B_0} is a diagonal matrix in the space-fixed frame.

$$\mathbf{I}_{B_0} = \frac{1}{4} m_B R_0^2 \begin{bmatrix} 1 & 0 & 0 \\ 0 & 1 & 0 \\ 0 & 0 & 2 \end{bmatrix} \quad (13)$$

Dynamic simulations of the Kresling structure are performed using ODE45 in MATLAB, with the state vector:

$$\mathbf{x} = \begin{bmatrix} \mathbf{r}_{B_0/A_0} \\ \boldsymbol{\Theta} \\ \dot{\mathbf{r}}_{B_0/A_0} \\ \boldsymbol{\omega}_B \end{bmatrix} \quad (14)$$

and its time derivative computed as

$$\dot{\mathbf{x}} = \begin{bmatrix} \dot{\mathbf{r}}_{B_0/A_0} \\ \mathbf{R}_{\omega_B}^{-1} \boldsymbol{\omega}_B \\ \ddot{\mathbf{r}}_{B_0/A_0} \\ \dot{\boldsymbol{\omega}}_B \end{bmatrix} \quad (15)$$

The last two components of Equation (15) are computed from Equation 12. While the above equations are developed for a single Kresling module, they may be extended to the structures

composed of multiple layers, as in Figure 1, by including the influence of trusses connecting both adjacent modules when computing forces in Equation 5. For the multi-module case, the state vector \mathbf{x} has $12n_m$ entries, where n_m is the number of modules.

QUASI-STATIC ANALYSIS

Structures based on Kresling geometry exhibit a wide range of interesting mechanical properties, including bistability and near-zero stiffness [7,20]. In the context of deployable structures applications, it is critical to consider the energy landscapes of such structures to understand the stability characteristics and determine the activation energy required to transform or reconfigure the system from one shape to another. Kresling structures have a large design space, and different mechanical behaviors can be achieved by varying geometric parameters such as the number of vertices n , the natural height h_0 , and radius R_0 . In order to focus the present study on the key characteristics of multistability and tunable energy barriers, the design space considered here is limited to variations in the initial rotation γ_0 . The other nominal parameters are listed in Table 1.

TABLE 1. KRESLING MODULE PARAMETERS EMPLOYED IN ANALYSES

n	h_0 [m]	R_0 [m]	k_a, k_b [N/m]	m [kg]	c_a, c_b [N.s/m]
8	0.06	0.055	1000	0.1	20

Deployment paths

Quasi-static simulations are conducted with prescribed vertical displacements r_z , which is in the E_3 direction as indicated in Figure 4. All other coordinates are unconstrained. For the geometric parameters considered in this research, these quasi-static simulations only cause variation in γ . This indicates that under uniaxial transformation from the collapsed to fully deployed states, there is no loss of stability in off-axis directions. For example, Figure 5(a) shows the local minimum energy path on the (r_z, γ) plane for a module with a natural rotation angle $\gamma_0 = 32^\circ$ starting in its nominal configuration. As the module is compressed, the rotation angle increases and reaches a maximum of 41° at a full compression of $r_z = 0$. While this path tracks a local energy minimum, the trusses do deform, as shown in Figure 5(b). Both trusses are undeformed and have zero strain energy at the module $r_z = h_0$. As the module is compressed from its natural height, the vertical truss a contracts while the diagonal truss b extends. On the other hand, expansions of the module from its natural state along the minimum energy path results in an extension of truss a and a contraction of truss b .

Strain energy landscapes

The strain energy along the minimum energy path shown in Figure 5(a) is presented in Figure 6(a). The global energy minimum at $r_z = h_0$ is clearly visible, yet the system also appears to have a second local minimum, and hence a second stable configuration, at $r_z = 0$. This is an example of *asymmetric bistability* – the stable state to $r_z = 0$ is at a much higher energy

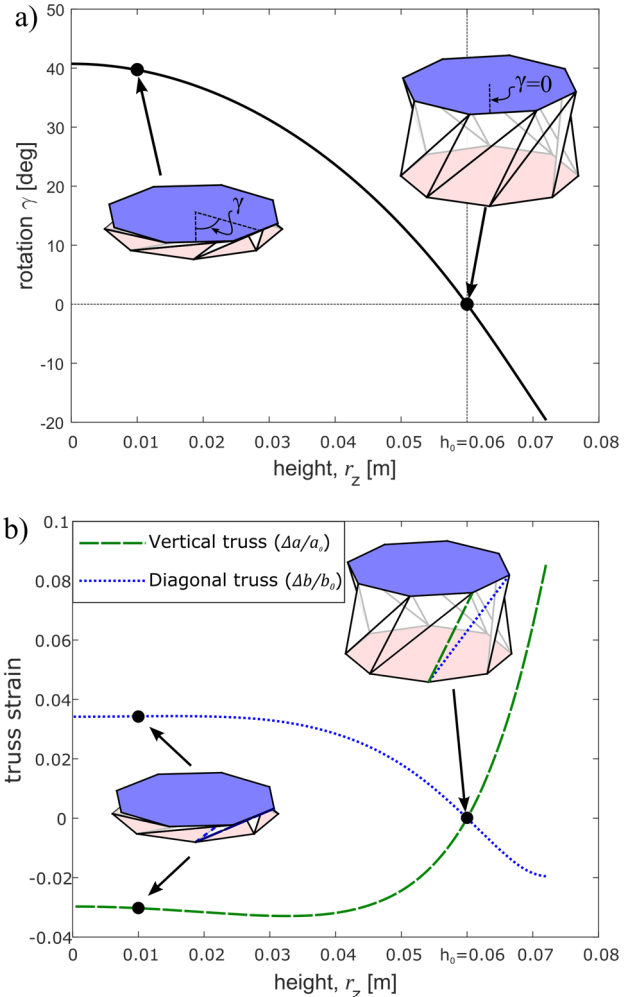


FIGURE 5. (a) ROTATION γ UNDER QUASI-STATIC VARIATION OF HEIGHT r_z FOR A KRESLING MODULE WITH AN INITIAL NATURAL ROTATION $\gamma_0 = 32^\circ$. ALL OTHER GEOMETRIC PARAMETERS ARE AS DEFINED IN TABLE 1. (b) DEFLECTION OF THE VERTICAL AND DIAGONAL TRUSS ALONG THE MINIMUM ENERGY PATH SHOWN IN (a).

level than stable state at $r_z = h_0$. A transition from one state to another necessitates overcoming the local energy maximum between the two states. Due to the asymmetry, much less energy is required to activate a deployment from the collapsed to the expanded state than to compress the module from the expanded state. Several qualitatively distinct energy landscapes arise as the parameter γ_0 is varied. Figures 6(b)-(d) present three other examples. Figure 6(b) presents the energy landscape for $\gamma_0 = 49.5^\circ$, which, like Figure 6(a), has energy minima at $r_z = 0$ and $r_z = h_0$. However, both states have zero energy, denoting *symmetric bistability*. As γ_0 is further increased to 53° , symmetric bistability is again observed, although the first energy minimum moves to $r_z = \frac{h_0}{2} = 0.03$ m. Hence, this partially deployed state may be sustained without the need for external constraining force. Lastly, Figure 6(d) presents a case in which there are two closely spaced energy minima, one at $r_z = h_0$ and

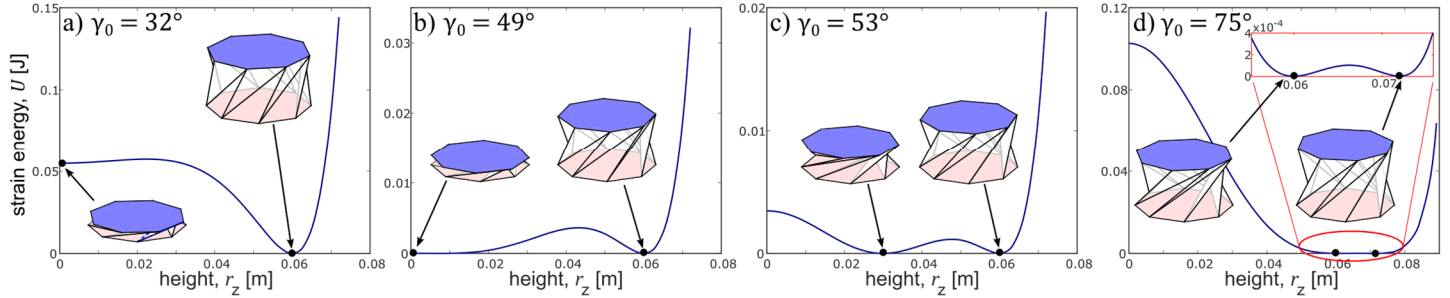


FIGURE 7. (a) STRAIN ENERGY LANDSCAPE ALONG THE UNIAXIAL DEPLOYMENT PATH FOR A MODULE WITH $\gamma_0 = 32^\circ$. THERE IS ONE GLOBAL ENERGY MINIMUM AT $r_z = h_0 = 0.06\text{m}$, AND A LOCAL MINIMUM AT $r_z = 0$. (b) FOR $\gamma_0 = 49^\circ$, THE CONFIGURATION AT $r_z = 0$ IS ALSO A GLOBAL ENERGY MINIMUM. (c) FOR $\gamma_0 = 53^\circ$, THIS SECOND MINIMUM IS AT AN INTERMEDIATE HEIGHT $r_z = h_0/2$. (d) FOR $\gamma_0 = 75^\circ$, THE SECOND ENERGY MINIMUM IS OBSERVED FOR $r_z > h_0$, INDICATED A STABLE HYPEREXTENDED STATE.

the other at $r_z > h_0$. This is in contrast to the other cases shown, since the second stable state is now observed at a height that is greater than the nominal natural height of the module.

In order to provide further insight into the influence of initial rotation γ_0 on the stability characteristics, Figure 7 presents a contour plot showing the strain energy stored in the truss elements of modules with different γ_0 as their height r_z is varied. Darker colors denote lower strain energy while lighter colors denote higher energy. Thick curves trace local minima of the contour, denoting stable states. There are several regions with qualitatively distinct behavior for the range of γ_0 studied. These regions are labeled and separated by dark vertical lines. When $\gamma_0 < 24^\circ$, the structure exhibits only one stable state at its natural height h_0 . Thus, this region is denoted the *monostable* range. For $24^\circ < \gamma_0 < 49^\circ$, a local energy minimum at $r_z = 0$ is observed, and the module is *asymmetrically bistable*. The specific case presented in Figure 6(a) lies in this region. In this region, the stable configuration at $r_z = 0$ has some quantity of strain energy stored in the truss elements. Hence transition from the collapsed state to the zero-energy expanded state of the module requires overcoming a smaller energy barrier than the reverse transition back to the collapsed state. At $\gamma_0 = 49^\circ$, $r_z = 0$ becomes a local energy maximum, marking a bifurcation point. At this bifurcation point, the fully compressed state has zero energy, as presented in Figure 6(b). For $49^\circ < \gamma_0 < 67.5^\circ$, there are two global minima with zero strain energy. One is located at the natural height $r_z = h_0$ and another at some *intermediate* height $0 < r_z < h_0$. At $\gamma_0 = 67.5^\circ$, the two local energy minima coalesce at $r_z = h_0$. This merging of the two roots is the origin for the zero stiffness mode reported in [20]. At initial rotations $\gamma_0 > 67.5^\circ$, the second stable state is observed at heights that exceed the nominal height of the module, and this region is hence deemed to have a stable *hyperextended* state.

The rich diversity of mechanical properties expressed by Kresling modules offers great potential for the development of deployable structures. For example, varying the parameter γ_0 within the stable intermediate range would allow a designer to tune the heights of the module's stable configurations. On the other hand, variations within the asymmetric region result in different energy barriers between the collapsed and extended state, allowing for a deployable structure that balances the need

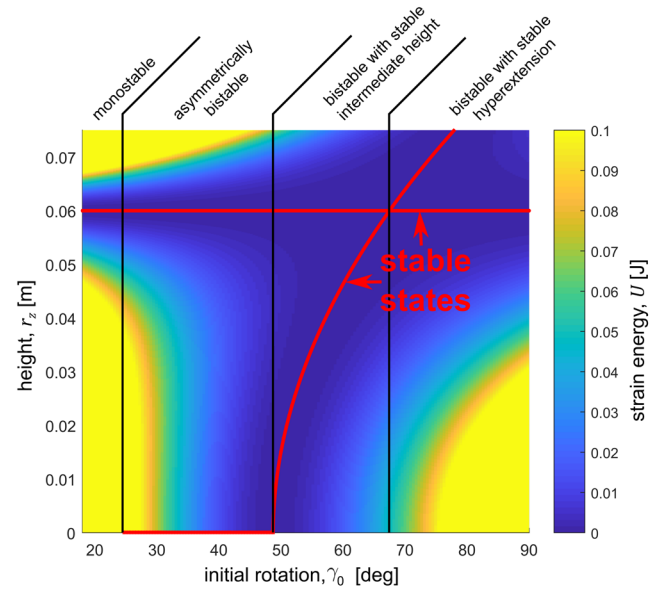


FIGURE 6. STRAIN ENERGY STORED IN THE TRUSS ELEMENTS OF KRESLING MODULES WITH DIFFERENT γ_0 , AS THEIR HEIGHT r_z IS VARIED ALONG THE MINIMUM ENERGY DEPLOYMENT PATH. STABLE CONFIGURATIONS, AT LOCAL ENERGY MINIMA, ARE INDICATED BY THE THICK CURVES, WHILE REGIONS OF QUALITATIVELY DISTINCT BEHAVIORS ARE SEPARATED BY VERTICAL LINES.

to minimize the energy required to activate such a transition while ensuring that the barrier is sufficiently high to avoid inadvertently triggering the configuration change [24].

DYNAMIC ANALYSIS

Origami-inspired structures are often designed to reconfigure quickly [6,19], hence the quasi-static investigations in the prior section are insufficient to properly understand their full features without complementary dynamic analyses [25,26]. In particular, quasi-static analyses of such structures implicitly assume that transformations will follow a minimum energy path,

as in Figures 5 and 6. However, dynamic loads may give rise to other motions [25]. For the Kresling structure considered in this research, quasi-static analyses of deployment were limited to the axial degrees of freedom r_z and γ , while the other coordinates were unperturbed. In this section, deployment dynamics are first explored with only the axial motions excited. Then, off-axis perturbations are deliberately introduced in order to study the robustness of the deployment process to such disturbances.

Axial Deployment

The parameter range of the Kresling structure considered in Figure 7 gives rise to several regions with qualitatively distinct mechanical behaviors, and each region may require a different strategy for system deployment. For example, structures in the monostable region have only one stable topology – at the natural deployed length of $r_z = h_0$. In this parameter region, the Kresling structure may be constrained and transported in a compressed configuration. When the constraint is released, the system will naturally expand and release the stored elastic energy, settling in the final deployed state. This scenario is depicted in Figure 8 for (a) a single module and (b) four serially connected modules with $\gamma_0 = 22^\circ$. Snapshots of intermediate times during the deployment process are also shown. A small amount of overshoot is observed in both cases and the system quickly settles to its final state. This behavior is reasonable, since the damping coefficients are chosen such that critical damping is achieved when a module is supported solely by vertical trusses.

If γ_0 is selected such that the structure is in the asymmetrically bistable region, deployment from its compressed state requires some energy to be provided to the system to overcome the energy barrier. Figure 9 shows deployment of (a) a single module and (b) a four-module structure with $\gamma_0 = 32^\circ$, and where the last element is provided an initial velocity $\dot{r}_z = 0.5 \frac{m}{s}$. This small impulse is sufficient to cause full deployment of the structure due to the small energy difference between $r_z = 0$ and the local maximum between the two stable states seen in Figure 6(a). For the four-module case, the deployment appears to occur sequentially. The top layer expands first, while the first layer expands last. A small overshoot is noted in the transient response for both the single module and four-module cases. One advantage to employing asymmetric bistability for deployment applications is that the structure can remain stable in its folded, compressed state without the need for additional constraining forces. However, this feature must be considered against the practicality of providing the structure with the sufficient activation energy necessary to ensure full deployment.

Robustness to off-axis motions

Although the dynamic analyses presented in the prior section have included all six degrees of freedom for each module, only axial motions are activated. In practice, out-of-axis motions may be perturbed for a variety of reasons, including imperfections in fabrication, the influence of gravitational and other inertial forces, or disturbances from the environment. In order to provide some initial insight into the performance of

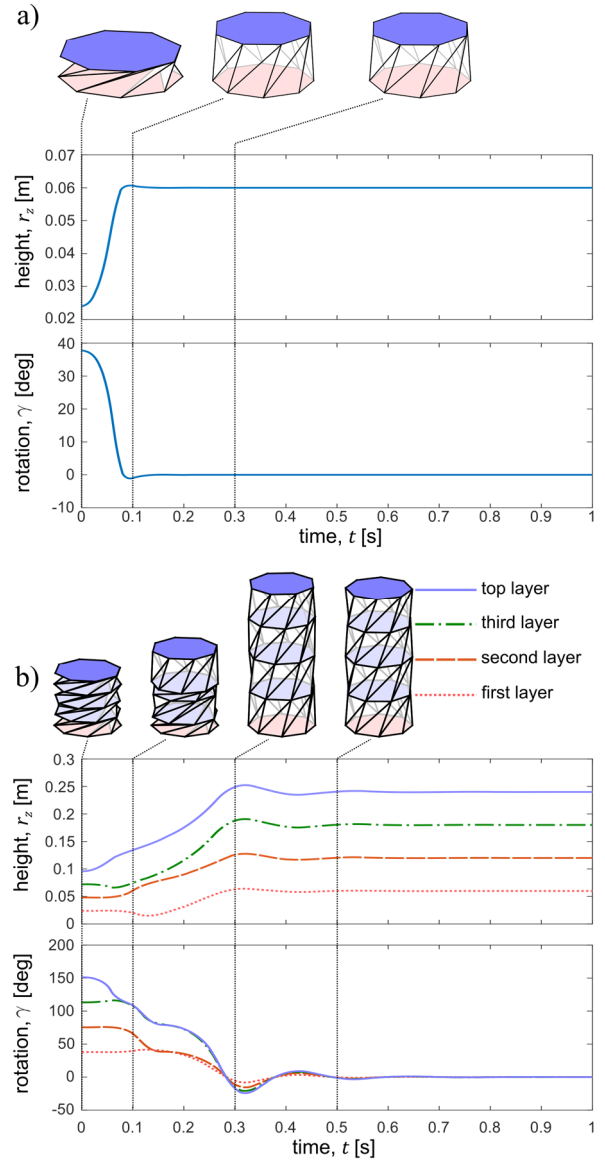


FIGURE 8. (a) HEIGHT AND ROTATION ANGLE DURING DYNAMIC DEPLOYMENT OF A KRESLING MODULE WITH $\gamma_0 = 22^\circ$. THE MODULE IS DEPLOYED USING THE ENERGY STORED IN ITS COMPRESSED STATE, AND SETTLES TO ITS STABLE EQUILIBRIUM AT $r_z = h_0 = 0.06\text{m}$. (b) DYNAMIC DEPLOYMENT OF A FOUR-MODULE STRUCTURE WITH $\gamma_0 = 22^\circ$ FOR ALL MODULES. SNAPSHOTS SHOW THE STATES BEFORE, DURING, AND AFTER DEPLOYMENT.

Kresling structures to off-axis perturbations, Figure 10 presents the transient response of a module with $\gamma_0 = 52^\circ$, which is in the *stable intermediate* range depicted in Figure 7. The structure is initially in its compressed configuration and provided an initial axial velocity $\dot{r}_z = 0.5 \frac{m}{s}$. In addition, there is a large off-axis initial angular velocity of $\omega_{B_2} = 10\pi \frac{\text{rad}}{\text{s}}$. Images above the plot show snapshots at selected times. The influence of the initial off-

axis angular velocity results in a perturbation of $\alpha, \beta, r_x,$ and r_y . The snapshot at time $t = 0.02s$ clearly shows that non-axial degrees of freedom are excited. However, this off-axis motion dies out much more quickly than the axial extension and rotation

r_z and γ , suggesting some degree of robustness to such perturbations.

To gain further insight, an analysis of the structure's modes is conducted. The system is linearized around the deployed configuration at $r_z = h_0$ by assuming small motions. Under this assumption, the Euler angle rates $\dot{\Theta}$ are approximately equal to the components of angular velocity ω . A mass matrix M is constructed, and the partial derivatives of the force and torque in Equations (5) and (11) are computed to obtain a 12x12 local stiffness matrix K .

$$M = \begin{bmatrix} mI_3 & \mathbf{0} \\ \mathbf{0} & I_{B_0} \end{bmatrix} \quad (16a)$$

$$K = \begin{bmatrix} \frac{\partial F}{\partial r_{B_0/A_0}} & \frac{\partial F}{\partial \Theta} \\ \frac{\partial T}{\partial r_{B_0/A_0}} & \frac{\partial T}{\partial \Theta} \end{bmatrix} \quad (16b)$$

where I_3 is the 3x3 identity matrix.

Consequently, the eigenvalue problem can be solved to yield the natural frequencies and mode shapes. The first three modes are shown in Figure 11. The fundamental mode, at $\omega_1 = 3.94$ Hz, only has components of axial displacement r_z and axial rotation γ . The second and third modes, at $\omega_2 = \omega_3 = 9.45$ Hz,

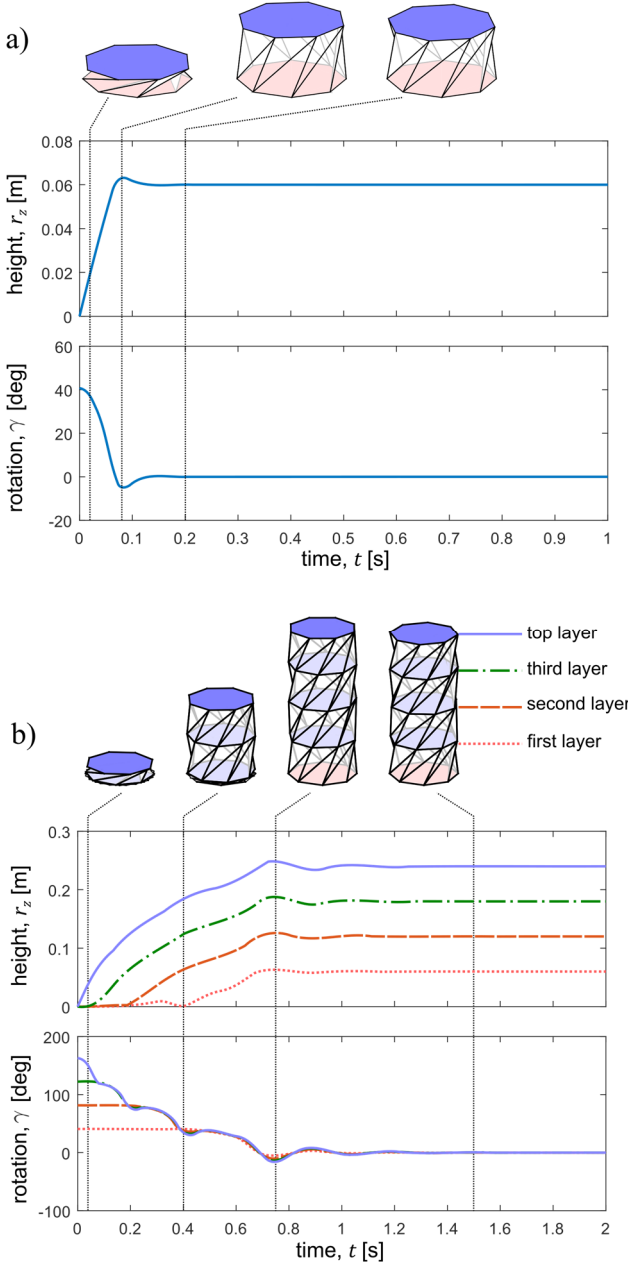


FIGURE 9. (a) HEIGHT AND ROTATION ANGLE DURING DYNAMIC DEPLOYMENT OF A KRESLING MODULE WITH $\gamma_0 = 32^\circ$. THE MODULE IS DEPLOYED BY PROVIDING AN INITIAL VELOCITY $\dot{r}_z = 0.5$ m/s TO THE LAST ELEMENT, AND SETTLES TO ITS STABLE EQUILIBRIUM AT $r_z = h_0 = 0.06$ m. (b) DYNAMIC DEPLOYMENT OF A FOUR-MODULE STRUCTURE WITH $\gamma_0 = 22^\circ$.

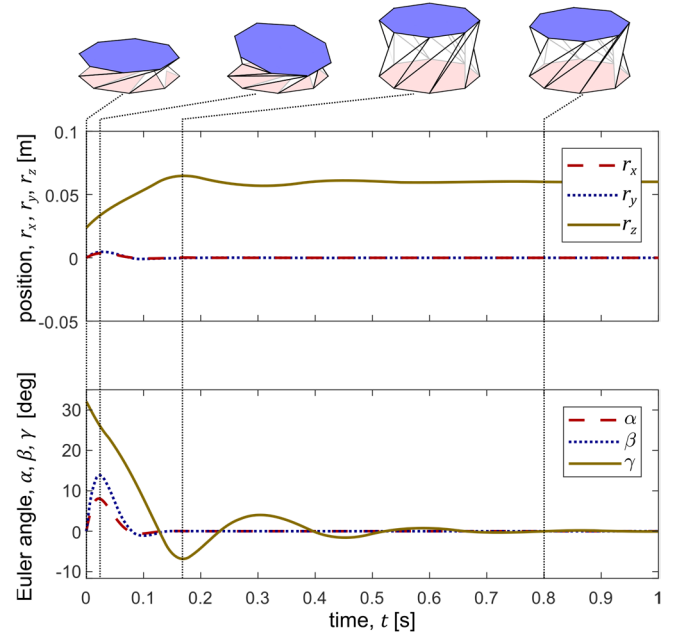


FIGURE 10. TRANSIENT RESPONSE OF A MODULE WITH $\gamma_0 = 52^\circ$ FROM AN INITIALLY COMPRESSED STABLE STATE WITH AN INITIAL AXIAL VELOCITY $\dot{r}_z = 0.5$ m/s AND A LARGE OFF-AXIS ANGULAR VELOCITY COMPONENT $\omega_{B_2} = 10\pi$ rad/s. THE OFF-AXIS PERTURBATION IS CLEARLY NOTED IN THE SNAPSHOT FOR $t = 0.02s$, BUT ITS INFLUENCE QUICKLY DIMINISHES, SUGGESTING A ROBUSTNESS TO SUCH OFF-AXIS PERTURBATIONS DURING DEPLOYMENT.

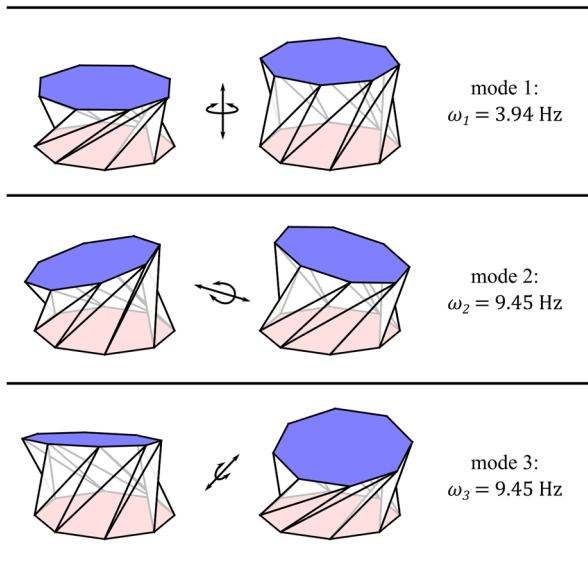


FIGURE 11. FIRST THREE LINEARIZED MODES IN THE DEPLOYED CONFIGURATIONS FOR A MODULE WITH $\gamma_0 = 52^\circ$. THE FIRST MODE, CORRESPONDING TO AXIAL DISPLACEMENT r_z COUPLED WITH AXIAL ROTATION γ IS AT A MUCH LOWER FREQUENCY THAN THE HIGHER MODES, WHICH DENOTE ORTHOGONAL, OFF-AXIS MOTIONS.

denote off-axis motions in the r_x , r_y , α , and β directions, and are thus uncoupled from axial motions. Since the off-axis modes have a much higher natural frequency, they tend to be dissipated much more quickly, resulting in the behavior observed in Figure 10. This result suggests that Kresling structures are capable of reliable deployment in the desired axial direction while being resistant to disturbances in other directions.

CONCLUSIONS

This research explores the rich mechanics and dynamic response of Kresling origami-inspired structures, with specific focus on their behavior during deployment. A truss model is developed that captures the full six-degree-of-freedom motion of a Kresling module, including off-axis motions that have often been ignored in previous study. Then, a quasi-static analysis is conducted of Kresling structures with varying geometry, revealing several qualitatively distinct behaviors that can be achieved by tuning the initial rotation angle of the module. The structure is monostable for small initial rotation angles, and its only stable configuration is at its fully deployed length. As the initial rotation angle is increased, the structure exhibits asymmetric and symmetric bistability, while extremely large rotation angles give rise to a stable *hyperextended* state beyond the structure's natural length. For each case, a different deployment strategy may be preferred. For example, a monostable structure can be deployed by releasing a constraining force that keeps the system in its collapsed configuration, allowing it to naturally expand and settle in its deployed state. On the other hand, bistable designs require an initial activation

energy to overcome a local energy maximum between stable states but do not need a constraining force to remain in the compressed configuration.

The dynamic response of a Kresling structure during deployment shows robustness to out-of-axis motions, even when deployment occurs quickly. In order to gain further insight into this behavior, a linearized analysis is conducted, revealing that the axial and non-axial motions are decoupled. Furthermore, the lowest natural frequencies corresponding to off-axis motions are significantly higher than those for axial motions. Hence, off-axis disturbances are dissipated much more quickly, as demonstrated by transient analyses. The findings illustrate that Kresling origami-inspired systems demonstrate great potential for a range of deployable structure applications. Rich mechanical properties can be achieved by tuning relatively simple geometric parameters, while their dynamic response shows robustness to perturbations and disturbances in directions orthogonal to the desired deployment stroke. Ongoing work is on exploring the use of different models to accurately reflect the stretching and bending behavior of folded Kresling structures, as well as experimental validation of the findings in this research.

ACKNOWLEDGEMENTS

This research is supported by the National Science Foundation under grant number 1634545, and the University of Michigan Collegiate Professorship.

REFERENCES

- [1] Lebée, A., 2015, "From Folds to Structures, a Review," *Int. J. Sp. Struct.*, **30**(2), pp. 55–74.
- [2] Schenk, M., and Guest, S. D., 2011, "Origami Folding: A Structural Engineering Approach," *Origami 5 Fifth Int. Meet. Origami Sci. Math. Educ.*, pp. 1–16.
- [3] Felton, S., Tolley, M., Demaine, E. D., Rus, D., and Wood, R., 2014, "A Method for Building Self-Folding Machines," *Science*, **345**(6197), pp. 644–646.
- [4] Natori, M. C., Katsumata, N., Yamakawa, H., Sakamoto, H., and Kishimoto, N., 2013, "Conceptual Model Study Using Origami for Membrane Space Structures - a Perspective of Origami-Based Engineering," *IDETC/CIE 2013*, Portland, OR, USA.
- [5] Miura, K., 1985, "Method of Packaging and Deployment of Large Membranes in Space," *31st Congress of the International Astronautical Federation*, Tokyo.
- [6] Thrall, A. P., and Quaglia, C. P., 2014, "Accordion Shelters: A Historical Review of Origami-like Deployable Shelters Developed by the US Military," *Eng. Struct.*, **59**, pp. 686–692.
- [7] Zhai, Z., Wang, Y., and Jiang, H., 2018, "Origami-Inspired, on-Demand Deployable and Collapsible Mechanical Metamaterials with Tunable Stiffness.," *Proc. Natl. Acad. Sci. U. S. A.*, **0**, p. 201720171.
- [8] Filipov, E. T., Liu, K., Tachi, T., Schenk, M., and Paulino, G. H., 2017, "Bar and Hinge Models for Scalable Analysis of Origami," *Int. J. Solids Struct.*, **124**,

- pp. 26–45.
- [9] Fang, H., Chu, S. C. A., Xia, Y., and Wang, K. W., 2018, “Programmable Self-Locking Origami Mechanical Metamaterials,” *Adv. Mater.*, **30**(15), pp. 1–9.
- [10] Filipov, E. T., Tachi, T., and Paulino, G. H., 2015, “Origami Tubes Assembled into Stiff, yet Reconfigurable Structures and Metamaterials,” *Proc. Natl. Acad. Sci.*, **112**(40), pp. 12321–12326.
- [11] Fang, H., Wang, K. W., and Li, S., 2017, “Asymmetric Energy Barrier and Mechanical Diode Effect from Folding Multi-Stable Stacked-Origami,” *Extrem. Mech. Lett.*, **17**, pp. 7–15.
- [12] Tachi, T., 2009, “One-DOF Cylindrical Deployable Structures with Rigid Quadrilateral Panels,” *Proceedings of the International Association for Shell and Spatial Structures (IASS) Symposium*, Valencia, pp. 2295–2305.
- [13] Liu, K., and Paulino, G. H., 2017, “Nonlinear Mechanics of Non-Rigid Origami: An Efficient Computational Approach,” *Proc. R. Soc. A Math. Phys. Eng. Sci.*, **473**, p. 20170348.
- [14] Faber, J. A., Arrieta, A. F., and Studart, A. R., 2018, “Bioinspired Spring Origami,” *Science*, **359**(6382), pp. 1386–1391.
- [15] Yoshimura, Y., 1955, “Mechanism of Buckling of a Circular Cylindrical Shell under Axial Compression,” *NASA TM 1390*, pp. 1–45.
- [16] Guest, S. D., and Pellegrino, S., 1996, “The Folding of Triangulated Cylinders, Part III: Experiments,” *J. Appl. Mech.*, **63**(1), p. 77.
- [17] Kresling, B., 2012, “Origami-Structures in Nature: Lessons in Designing ‘Smart’ Materials Biruta,” *Materials Research Society Symposium Proceedings*.
- [18] Cai, J., Deng, X., Zhou, Y., Feng, J., and Tu, Y., 2015, “Bistable Behavior of the Cylindrical Origami Structure with Kresling Pattern,” *J. Mech. Des.*, **137**(6), p. 061406.
- [19] Pagano, A., Yan, T., Chien, B., Wissa, A., and Tawfick, S., 2017, “A Crawling Robot Driven by Multi-Stable Origami,” *Smart Mater. Struct.*, **26**(9).
- [20] Yasuda, H., Tachi, T., Lee, M., and Yang, J., 2017, “Origami-Based Tunable Truss Structures for Non-Volatile Mechanical Memory Operation,” *Nat. Commun.*, **8**(1), pp. 1–6.
- [21] Wilson, L., Pellegrino, S., and Danner, R., 2013, “Origami Sunshield Concepts for Space Telescopes,” *54th AIAA/ASME/ASCE/AHS/ASC Struct. Struct. Dyn. Mater. Conf.*
- [22] Yasuda, H., Miyazawa, Y., Charalampidis, E. G., Chong, C., Kevrekidis, P. G., and Yang, J., 2018, “Origami-Based Impact Mitigation via Rarefaction Solitary Wave Creation,” *arXiv Prepr.*, pp. 1–19.
- [23] O’Reilly, O. M., 2008, *Intermediate Dynamics for Engineers: A Unified Treatment of Newton-Euler and Lagrangian Mechanics*, Cambridge University Press, Cambridge, UK.
- [24] Kidambi, N., Harne, R. L., and Wang, K. W., 2017, “Energy Capture and Storage in Asymmetrically Multistable Modular Structures Inspired by Skeletal Muscle,” *Smart Mater. Struct.*, **26**(8), p. 085011.
- [25] Liu, C., and Felton, S. M., 2018, “Transformation Dynamics in Origami,” *Phys. Rev. Lett.*, **121**(25), p. 254101.
- [26] Fang, H., Li, S., Ji, H., and Wang, K. W., 2017, “Dynamics of a Bistable Miura-Origami Structure,” *Phys. Rev. E*, **052211**, pp. 27–29.